Journal of Natural Gas Science and Engineering 26 (2015) 1317–1331

Contents lists available at ScienceDirect

Journal of Natural Gas Science and Engineering

journal homepage: www.elsevier.com/locate/jngse

Using differential evolution for compositional history-matching of a tight gas condensate well in the Montney Formation in western Canada

Hamidreza Hamdi [a, *], Hamid Behmanesh [b], Christopher R. Clarkson [c], Mario Costa Sousa [a]

[a] Department of Computer Science, University of Calgary, Canada
[b] Department of Chemical and Petroleum Engineering, University of Calgary, Canada
[c] Department of Geoscience, University of Calgary, Canada

ARTICLE INFO

Article history:
Received 19 May 2015
Received in revised form
5 August 2015
Accepted 6 August 2015
Available online 11 August 2015

Keywords:
Tight gas reservoir
Compositional simulation
History matching
Differential evolution
Sensitivity indices

ABSTRACT

Production data analysis for low-permeability unconventional reservoirs is a challenging task, particularly for cases where multi-phase flow occurs within the reservoir. Analytical models developed to account for multi-phase flow typically require calculation of pseudo variables, which in turn require knowledge of relative permeability and fluid data. In the presence of sparse sampling, the analytical models often do not provide satisfactory results when there are so many unknown parameters. In such situations, numerical models are better suited, using a history matching framework to assist with reservoir and fluid characterization.

In this work, we implement an assisted history-matching routine to characterize reservoir fluids and extract reservoir and hydraulic fracture properties for a hydraulically-fractured horizontal well completed in a tight gas condensate reservoir within the Montney Formation in western Alberta, Canada. The initial water distribution (e.g. movable water profile in the reservoir), *in situ* fluid (e.g. initial hydrocarbon composition with C_{7+} properties) and reservoir properties (e.g. permeability in the matrix and around the fracture, and pressure dependent fracture permeability) are described in terms of 20 unknown parameters, which creates a high-dimensional inverse problem. We use the Differential Evolution algorithm, which is a powerful population-based optimization algorithm, and employ numerical compositional simulations to match pressure, water and hydrocarbon rates, and surface compositions of the produced fluids. Application of this optimization routine results in a good match to all measured data. The DE algorithm is repeated for an extra run to check for the existence of other non-unique solutions. The history-match results helped determine parameters for well/reservoir description and develop a compositional fluid model based on the measured separator composition data. The collected samples for both DE runs, along with one thousand extra samples from quasi-random sequence sampling design, provide a pool of data with invaluable information that are used to perform the global sensitivity analysis and to rank the contribution of each descriptive parameter on the variances of the reservoir outputs. In this way, the value of production data and surface compositions for the characterization of reservoir and fluid is quantified.

This work aims to provide a practical and simple workflow for analysis of unconventional reservoirs where the direct analytical approaches cannot be applied.

1. Introduction

Unconventional reservoirs with ultra-low permeability, such as shales, while containing abundant hydrocarbon resources, are difficult to produce using conventional techniques. Commercial production from such reservoirs typically requires the drilling of long horizontal wells completed in multiple hydraulic fracturing stages (multi-fractured horizontal wells or MFHWs). The intent of hydraulic fracturing is to increase the contact between the ultra-low matrix volume and the conductive fractures; fracture geometry may be very complex, depending on the combination of in-situ

* Corresponding author.
E-mail address: hhamdi@ucalgary.ca (H. Hamdi).

http://dx.doi.org/10.1016/j.jngse.2015.08.015
1875-5100/

rock properties, stress and hydraulic fracture design. As a result, production to the MFHWs may be initially dominated by transient linear flow from the low-permeability matrix to the fractures (Nobakht and Clarkson, 2011, 2012; Nobakht and Mattar, 2012).

Production data analysis using analytical, semi-analytical and empirical approaches is commonly applied to shale and tight formations. However, numerical methods are superior to such methods as more physics can be involved for better understanding of the flow in porous media (Lee and Sidle, 2010; Kalantari Dahaghi et al., 2012). The details of numerical models depend on the purpose of study, and also the availability and complexity of the data to be integrated. Some models, i.e. integrated earth models (Fanchi, 2000, 2002), reflect the detailed geological, geomechanical and engineering data, whereas others are used as super-analytical (Houzé et al., 2011) or average models with enough complexity to address some important aspects of reservoir performance and uncertainty propagations. Numerical methods can be used in sensitivity analysis and parametric studies to understand the effect of different parameters such as fracture network properties and/or complex nonlinear effects (e.g. multi-phase flow, non-Darcy effects, or gas adsorption/desorption) on the performance of such reservoirs. Orangi et al. (2011) performed a sensitivity study using compositional simulations of shale oil and gas condensate fractured wells to evaluate the importance of fluid and rock properties for reservoir performance prediction. Fan et al. (2011) used dual porosity models to simulate the performance of vertical and horizontal wells in the Eagle Ford shale and to find the relationship between geological properties and production trends.

The use of numerical simulations for accurate predication of reservoir behavior requires assisted history matching methods to alter the model properties in an efficient way. Previous work on history matching of tight/shale reservoirs is mainly based on manual or deterministic methods to adjust the fracture networks and properties. Examples of such approaches are documented by Mayerhofer et al. (2006) and Cipolla et al. (2009) for the Barnett shale, and Bazan et al. (2010) for the Eagle Ford where discrete fracture network properties were modified deterministically to find the representative models. Although application of automatic assisted history matching techniques is now a standard procedure for many conventional reservoirs, its use for the unconventional reservoirs has been limited (Ghods and Zhang, 2010). Gorucu and Ertekin (2011) used Artificial Intelligence in dual porosity tight gas simulations to provide information about stimulation strategies and design parameters in transversely fractured horizontal wells. Yin et al. (2011) used the Genetic Algorithm (Mitchell, 1998) to calibrate their shale gas model by adjusting rock compaction, the stimulated reservoir volume close to the hydraulic fracture, and fracture properties. Kalantari Dahaghi et al. (2012) implemented Artificial Intelligence to create a proxy model in synthetic shale gas numerical models with complex fracture networks for fast evaluation of the reservoir performance. Bhattacharya and Nikolaou (2013) presented a statistical approach based on Principal Component Analysis (Jolliffe, 2002) to analyze historical production data from existing unconventional gas wells and to predict new well production profiles. Zhang and Fassihi (2013) presented a workflow for assisted history matching and uncertainity analysis of a multi-stage horizontal fractured shale oil well in the Eagle Ford reservoir using Genetic Algorithm and cluster analysis. They used three different geomodels with different probabilities and included the uncertainity in rock and fracture properties and also the bubble point pressure in their black oil simulations. Enyioha and Ertekin (2014) applied the Artificial Neural Network approach to map various well design parameters for multi-lateral wells in tight oil formations with multi-phase flow from synthetic models. Other history matching techniques such as the Ensemble Kalman Filter have also been implemented by Nejadi et al. (2014) to history match a shale oil well in Horne River Basin and to assess the uncertainty of Discrete Fracture Network properties (e.g. fracture density, fracture intensity, special distribution and fracture conductivity) and their impacts on the production profile.

Our literature survey reveals that the focus of many numerical studies for production analysis of unconventional tight and shale reservoirs has been largely on the impacts of rock and fracture uncertainties. However, for the case of multi-phase flow, the analysis can be complicated particularly when reliable fluid data and PVT models are not available. Therefore, for such cases, an extra dimension must be added to assisted history matching problems to include the impact of uncertainty in the fluid data on the matching process.

In this paper, we apply an assisted history-matching approach to a multi-fractured tight gas condensate well in the Montney Formation in western Alberta, Canada. The intent of these efforts are to derive hydraulic fracture and reservoir properties; further, and very importantly, we are able to derive a fluid model by matching not just fluid rates and pressures, but also fluid composition. The complexity of multi-phase flow in addition to very limited data, make the problem a challenging task to analyze. The available data include initial pressure from a DFIT (Diagnostic Fracture Injection Test) interpretation (Barree, 2013), flowing bottomhole pressure, surface fluid rates, and some surface fluid sample compositions. The novelty of the current work is in the combined use of compositional simulation with the Differential Evolution approach (Storn and Price, 1995; Price et al., 2005) to characterize the reservoir, hydraulic fracture and the *in situ* fluid composition. The workflow allows us to perform global sensitivity analysis (Saltelli, 2002) to rank the parameter importance in terms of reservoir production and composition data (Fig. 1). The value of data in reducing the uncertainty in the reservoir and fluid characterization is quantified. Although detailed multi-physics, multi-process modeling was not the purpose of this paper; the nonlinearity and high dimensionality of the problem made the subject case an excellent candidate for assisted history matching using a simplified average model.

This study provides an engineering workflow for setting up a simplified mathematical model and presenting a calibration method to assess the behavior of a low permeability gas condensate system. This, however, does not impact the generality of the approach where more information and other uncertain variables can be plugged into the inverse problem.

2. Use of differential evolution algorithm for history matching

History matching in reservoir engineering refers to matching dynamic field data such as flow rates and pressures with numerical or analytical reservoir models. This is an inverse problem and is achieved by perturbing the parameters that can describe the subject reservoir and well through an optimization algorithm. This process has some distinct steps, including parameterization, forward modeling and inversion (Tarantola, 2005). In the parameterization steps, some variables or processes that can adequately describe the model are selected. This step is the most important step which requires expert knowledge to analyze and select the elements of model description according to the purpose and availability of data. Obviously, in practical problems where the data are frequently sparse, multi-physics parameterization is not usually possible. Increasing the number of unknowns with limited constraints on each variable not only does not help enhance understanding of the reservoir performance, but also can unnecessarily complicate the problem. Therefore, parameterization can be

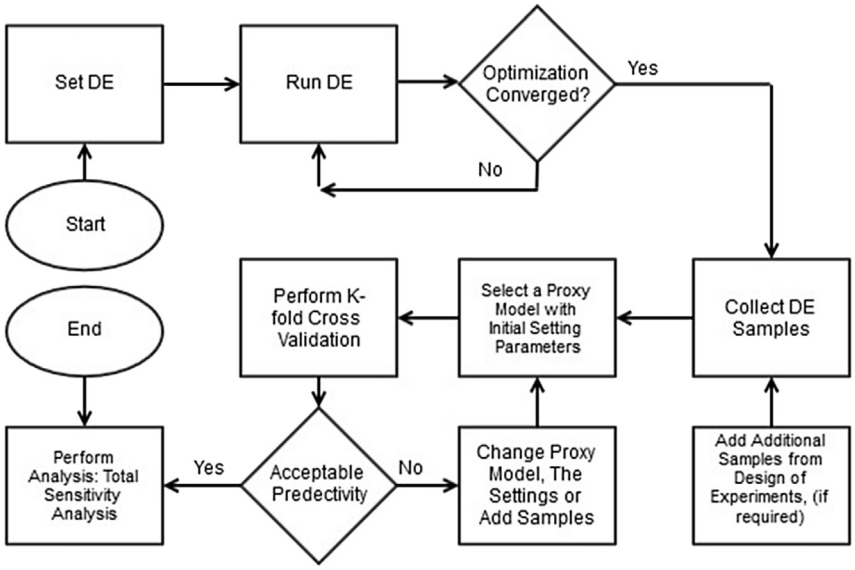

Fig. 1. Flowchart for optimization and global sensitivity analysis used in this study.

described as an engineering art to describe a model in a simple way with a minimum number of parameters for a specific purpose. The forward modeling step is basically a fluid flow reservoir simulation step (i.e. compositional simulation in our case) using a finite difference or finite element approach. Lastly, inversion can be described as an optimization step to mathematically perturb the reservoir model parameters in order to minimize the misfit between the real data and the model output.

There are many optimization algorithms which can be generally divided into two groups: gradient-based (Bard, 1974) and population-based sampling methods (Simon, 2013). The gradient-based methods, such as Newton Raphson (Atkinson, 1978), are based on function derivatives and are generally fast. However, they depend strongly on the starting point and don't have an extensive exploration view to find the global minima or maxima (Gilman and Ozgen, 2013). On the other hand, population-based methods are good at finding the global extrema from random or adaptive sampling of the parameter space. Contrary to gradient-based methods, the population-based methods use a population of samples at each iteration and can provide a set of solutions to the problem rather than a single point, and therefore can better address the non-uniqueness in solution for an inverse problem at a single trial. Approaches such as Differential Evolution (Storn and Price, 1995; Price et al., 2005), particle swarm optimization (Poli et al., 2007), ant colony optimization (Hajizadeh et al., 2009a) and sequential Bayesian Optimization (Jones et al., 1998; Jones, 2001; Hamdi et al., 2014) are some examples of the population-based optimization algorithm. In this paper, we use Differential Evolution in search of global solutions to describe a high dimensional engineering problem. Some of previous work of using DE in the history-matching problems include that of Decker and Mauldon (2006) for estimating fracture size and shape from trace data, Hajizadeh et al. (2009b) for history matching of an oil reservoir model, Mirzabozorg et al. (2013) for parameter estimation of a Steam Assisted Gravity Drainage (SAGD) model and that of Awotunde and Mutasiem (2014) for drilling time optimization.

Differential Evolution (DE) is a powerful population-based adaptive sampling approach to find the global extrema of a black box nonlinear model (Storn and Price, 1995; Price et al., 2005). This can be seen as an improved version of the well-known genetic algorithm (Mitchell, 1998) with a more involved mutation step and better exploration-exploitation of the parameter space (Epitropakis et al., 2008). There are many variants of DE. A basic variant of Differential Evolution (DE/BEST) starts with the evaluation of an initial population (with N_p members) from the parameter space (n_d-dimensional). Each member of the population is a vector randomly sampled from the parameter space that has honored the predefined parameter ranges. The positions of the population members are then ranked according to their misfit with real data. For each target vector $\mathbf{x}$, the current best member ($\mathbf{y}_{best}$), with a lowest misfit $f(\mathbf{y}_{best})$, and two other randomly selected distinct members ($\mathbf{y}_2$ and $\mathbf{y}_3$), are mutated and create a new mutant member ($\mathbf{v}_{G+1}$) as follows:

$$\mathbf{v}_{G+1} = \mathbf{y}_{best,G} + F\left(\mathbf{y}_{2,\,G} - \mathbf{y}_{3,G}\right) \quad (1)$$

where, subscript "G" is the current population or generation. "F" is called the step size or the scaling factor and is a real positive constant parameter ($F \leq 2$) that controls the rate with which the population evolves. The mutant member $\mathbf{v}$ is then compared with the vector member $\mathbf{x}$ (each element of vector $\mathbf{x}$ is shown by x_i). The mutant vector $\mathbf{v}$ and the member vector $\mathbf{x}$ in the population are then crossed over according to a preselected crossover probability constant ($CR \leq 1$) to generate a new vector $\mathbf{y}$. This is based on choosing a random number ζ between 1 and n_d (the dimension of the problem), and a random vector $\mathbf{r}$ with size of n_d. Each member of $\mathbf{r}$ is a random number r_i that is uniformly distributed between 0 and 1. The potential positions of the new vector $\mathbf{y} = [y_1, \ldots, y_i, \ldots, y_{nd}]$ are computed with the following logic: if $r_i < CR$ or $i = R$ (R is a random index between 1 and n_d) then $y_i = v_i$ otherwise $y_i = x_i$. If $f(\mathbf{y}) < f(\mathbf{x})$ then the target vector in the population (i.e. $\mathbf{x}$) is replaced with the newly generated member ($\mathbf{y}$) and a new population is created. This new population is called a generation and/or iteration.

This process is repeated until the maximum number of generations is reached. The choices of CR and F have the greatest impact on the convergence of the problem. However, according to the authors' experience with DE a $CR = 0.5$ and $F = 0.5$ can usually provide a good convergence rate in many reservoir engineering and well testing applications (Hamdi et al., 2015).

3. Study well description

The well analyzed in this study is completed in a tight gas condensate reservoir within the Montney Formation. The lower

Triassic Montney Formation, which is located in the Western Canadian Sedimentary Basin, hosts vast gas and oil resources within conventional and unconventional reservoirs (Zonneveld et al., 2011). The focus of the current study is in an area just west of the city of Fort St. John where the Montney is comprised mainly of shale and siltstone (Rokosh et al., 2012).

Fig. 2 from National Energy Board (2013) provides an areal map illustrating the various rock types in the Montney Formation. The expected fluid type distribution within the Montney in British Columbia is also shown in Fig. 3 (Adams, 2013). Liquids rich gas resources are expected in the northeastern portions of this mapped area, while dry gas is expected towards the southwest.

The subject well in this study is a lower Montney horizontal well that is 1520 m in length and is completed with 8 fracture stages at an average depth of 1984.2 m KB TVD (bottom toe perforation depth is 1974.8 m KB TVD and top heel perforation depth is 1993.6 m KB TVD). Production commenced in December 2012. The initial reservoir pressure was 4850 psi in December 2012, as determined from DFIT analysis. The flowing bottomhole pressure varied from near 4350 psi to 430 psi after around one year of production (Fig. 4A) and is approximately constant in the late times. The flowing bottomhole pressure data was estimated from the surface measurements (Beggs and Brill, 1973) and provided to us from the operator company. It was confirmed with the operator that the subject well was not suffering from any liquid loading effects during this production period. The condensate gas ratio (CGR) decreased over time from around 35 barrels per million standard cubic feet (bbl/MMscft) to a constant value of 4 bbl/MMscf (Fig. 4B). This observation is consistent with Whitson and Sunjerga (2012) who observed that a constant condensate gas ratio may be observed in some saturated LRS gas condensate reservoirs when the condensate mobility is limited within the reservoir. Later Behmanesh et al. (2014, 2015) analytically proved that CGR is also constant for the constant flowing bottomhole pressure cases even if the condensate is mobile within the reservoir. Although the CGR is low for the subject well, there are still some concerns that the well might exhibit retrograde behavior in the reservoir which could negatively impact production. Therefore, during the well production period, some separator gas and condensate samples were taken for fluid analysis. Late-time fluid samples are considered to be more reliable than early-time samples. Therefore, one of the main purposes of this study is to tune an equation of state (EOS) for

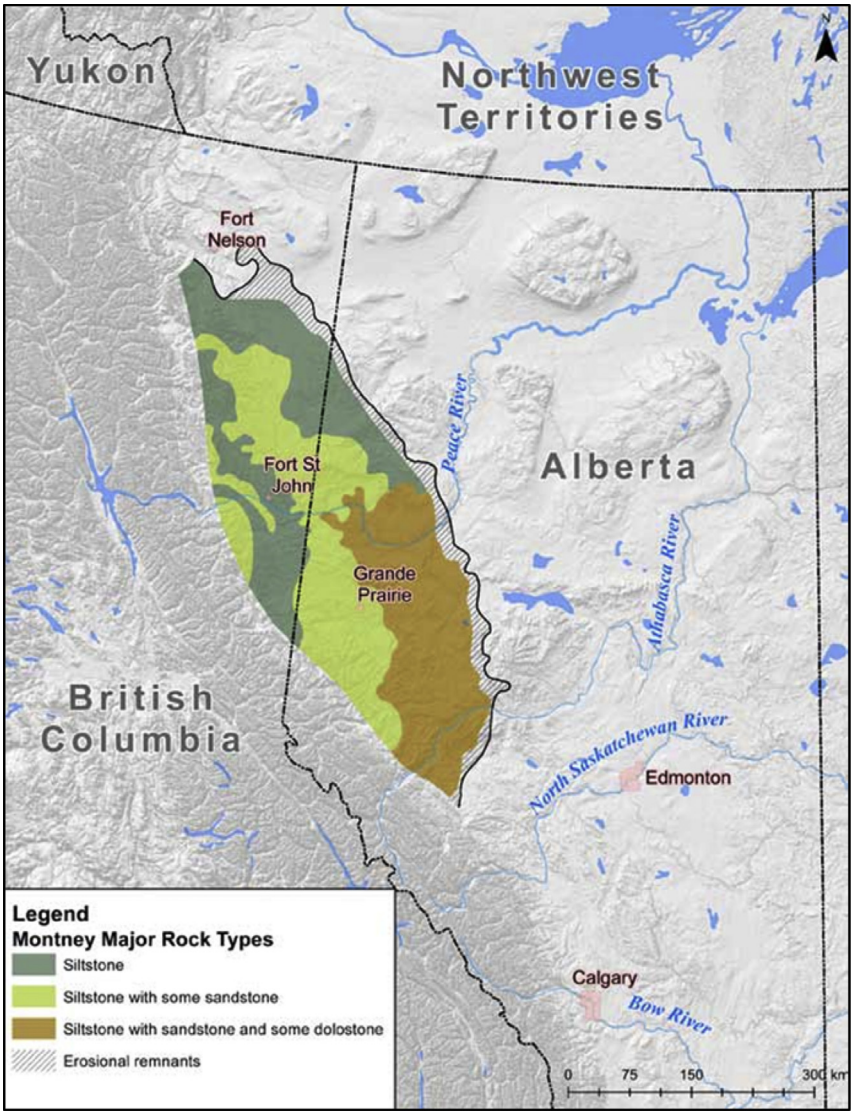

Fig. 2. Areal map of the Montney Formation in subsurface of Alberta and British Colombia with locations of different rock types (National Energy Board, 2013).

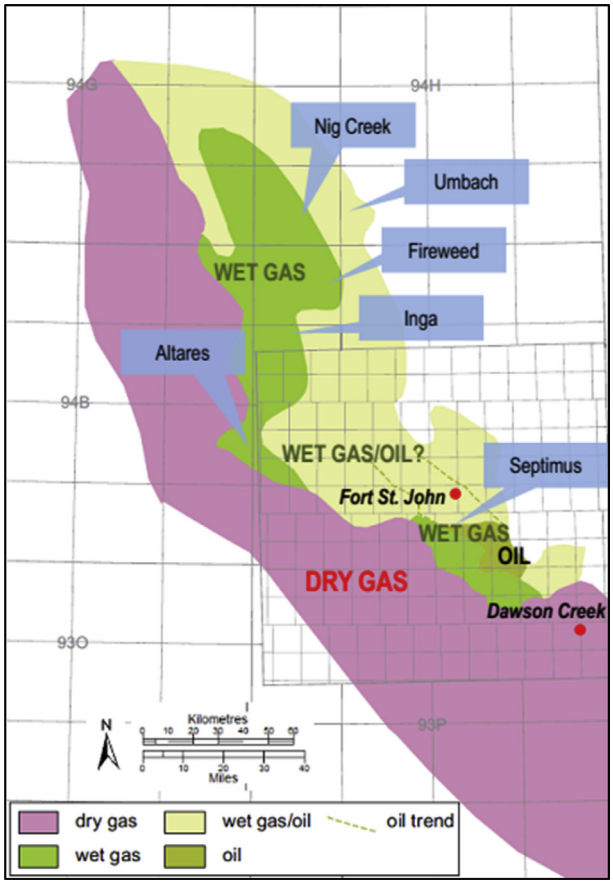

Fig. 3. The expected fluid distribution of the Montney Formation in British Columbia (Adams, 2013).

the *in situ* fluid in order to produce the same fluid compositions at a selected production time (100 days), when reliable stable samples were available. Table 1 provides the separator fluid compositions after 100 days of the production. This fluid cannot reliably represent the original fluid in the reservoir as compositional changes have probably occurred during production that must be verified by the compositional reservoir simulator. It should be noted that, contrary to the conventional tuning of an EOS from PVT analysis software, for liquid-rich unconventional reservoirs, the *in situ* reservoir fluid tuning by production data is affected by reservoir parameters such as permeability, adding to the uncertainty. Hence, a well history matching exercise with a reduced number of descriptive input parameters was intended to perform the parameter estimation for this highly nonlinear system.

4. Simulation model set-up

In this study, we have setup our numerical simulations to model transient linear flow to the hydraulic fractures. Evidence for the appearance of transient linear flow is provided in Fig. 5, where the normalized rate integral for the gas phase and its corresponding log derivative are plotted vs material balance time (Palacio and Blasingame, 1993). The plot exhibits a $-½$ slope indicative of transient linear flow for almost entire production period of the well.

Because we were only seeing linear flow (before fracture interference), and there was no evidence of other geological heterogeneities (such as faults or complex fracture distributions) affecting the rate-transient behavior, it was not possible for us at this stage to use more complex models without other supporting data. For numerical simulations we therefore created a one-dimensional (1D) single-fracture model, with a stimulated reservoir volume (SRV) surrounding it, to reproduce the transient linear flow signature observed in Fig. 5. The SRV is composed of a distribution of small-scale fractures resulting in an improved permeability region close to the primary fractures. The SRV permeability is a combination of the matrix and fracture permeabilities (Fisher et al., 2004; Mayerhofer et al., 2010; Mattar et al., 2011; Detring and Williams-Stroud, 2013). The SRV is frequently employed in engineering applications by defining few composite regions around the main hydraulic fracture to match the measured production data using analytical models (Stalgorova and Mattar, 2012a, b). The existence of this region near hydraulically fractured wells can be proved using the microseismic data (Albright and Pearson, 1982; Warpinski et al., 2004) and some recent studies, such as Maxwell et al. (2002, 2009), have attempted to characterize complex fracture geometry using such data. However, because of a lack of direct indicators, detailed knowledge of fracture network and spacing in the SRV is not possible. In this study, microseismic data were not available, and hence an inverse approach was used to find the SRV boundaries for this 1D problem.

Well performance was simulated using the CMG-GEM™ compositional reservoir simulator (CMG, 2014). Assuming symmetric and similar fracture stages, the overall production rates of the well were divided by 16 to simulate the flow towards one side of a single fracture face (Fig. 6). One dimensional (1D) reservoir grid cells in the y-direction were logarithmically propagated to accurately capture changes of pressure and saturation near the fracture face. Other simplifying assumptions in this study are summarized in Table 2.

Al Ghamdi and Ayala (2010) studied the effect of capillary pressure and relative permeability data on the performance of naturally fractured gas condensate reservoirs, and showed that the

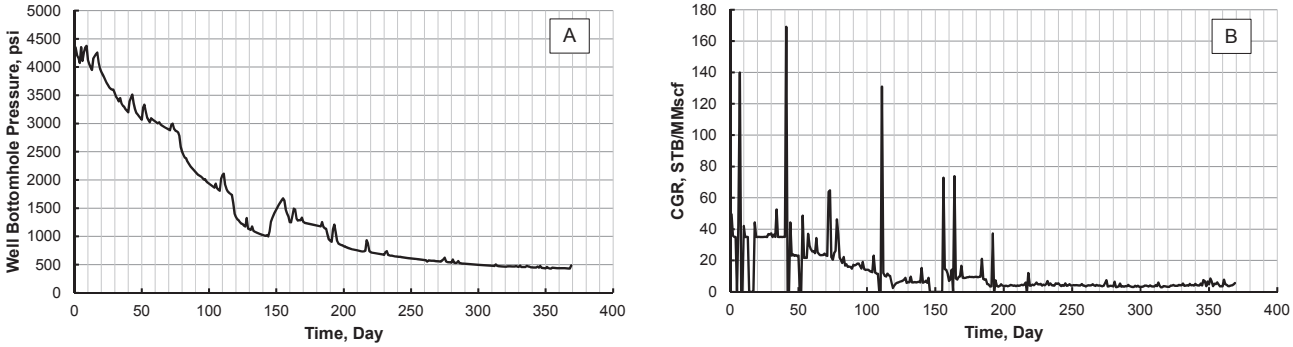

Fig. 4. Flowing bottomhole pressure and the condensate gas ratio for the study well.

Table 1
Separator oil and gas compositions for a fluid sample taken after 100 days of production.

Components	Separator liquid mole fraction, x_i	Separator gas mole fraction, y_i
N_2	nil	0.0011
CO_2	0.0003	0.002
C1	0.0552	0.8516
C2	0.0298	0.086
C3	0.0367	0.0305
iC4	0.0212	0.0073
nC4	0.044	0.01
iC5	0.0454	0.0039
nC5	0.0461	0.003
nC6	0.1253	0.0028
C_{7+}	0.596	0.0018

Table 2
The assumptions used for modeling linear flow towards the equivalent 1D fracture system.

Property	Value
Porosity, φ	0.05
Fracture Conductivity, $k_f \times w$	50 md ft
Reservoir thickness, h	328 ft
Fracture half-length[a], x_f	158.5 ft
Lateral-length[b], l	5000 ft
Capillary pressure	No
Non Darcy flow	No
Sorption	No
Flow regimes	Pure linear flow

[a] The combined effect of $x_f\sqrt{K}$ was simulated only through permeability variation and a constant x_f.
[b] To simulate pure transient linear flow.

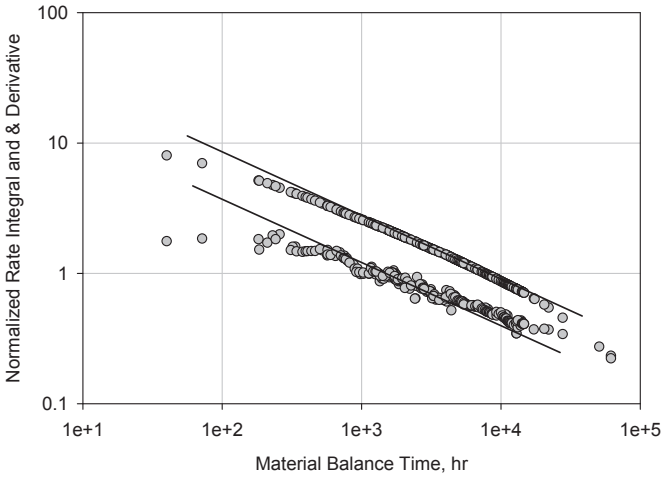

Fig. 5. Log–log plot of normalized rate integral and its corresponding log derivative vs material balance time t_e. The one half slope lines show the linear flow trend.

capillary pressure curves do not have a significant effect on the overall recovery compared relative permeability. Capillary effects are ignored in this study; however we note that the impact of water-gas capillary pressure on the after-injection induced fluid distribution is somewhat compromised by using an explicit initial fluid distribution in the model as explained in later sections. Non-Darcy flow due to slippage (Klinkenberg, 1941) in the matrix, and inertia (Forchheimer, 1901) in the hydraulic fractures were not considered at this stage of study.

Detailed geomechanical data were also not available for this study. However, because of the importance of geomechanical data, a simplified exponential fracture compaction model was implemented to modify the fracture transmissibility with changes in pressure.

As noted by Cipolla et al. (2010), gas desorption (Langmuir, 1916) can account for 5–15% of ultimate gas recovery, but has little impact on early production data. Hence, desorption effect was ignored in this study.

4.1. Parameters adjusted in simulation history-match

Twenty parameters were selected to represent the uncertainty in water saturation, rock, and fluid properties and are listed in Table 3. Ranges of parameters were developed through consultation with experts within the data provider company, an available database of similar wells in the subject field, and also by considering oil-gas recombination of the separator fluid at various CGR's.

4.1.1. Initialization

4.1.1.1. Water and rock. The simulation model was initialized using different initial water saturation profiles and permeability values. There is a considerable amount of water production (see Fig. 8D) since the start of production, which has a different salinity from the injected frac water. This might be indicative of initial mobile water in the system. A detailed numerical study of water injection and flow in shale reservoirs was performed by Jurus et al. (2013). Unfortunately, in this study, water injection data were not available to perform an analogous study. Therefore it was decided to explicitly initialize the reservoir model with a simplified mobile water profile as an uncertain parameter. A two-region (fracture and matrix) saturation profile was used to mimic the average water saturation within the SRV (S_{w_SRV}) and the lower average water saturation in the matrix reservoir volume (S_{w_init}). Therefore, we assume that the fractured region has an effective restricted volume around the hydraulic fracture with a high average volumetric water saturation due to water injection during hydraulic fracturing.

Permeability of the SRV and reservoir (matrix) rock were used as two separate matching parameters. The lateral extent of the SRV region is estimated from the overall remaining water in the reservoir after injection (Q_{w_r} = Volume of injected Water - Volume of produced water = 2245 bbl or 12,606 ft^3), which is given as follows:

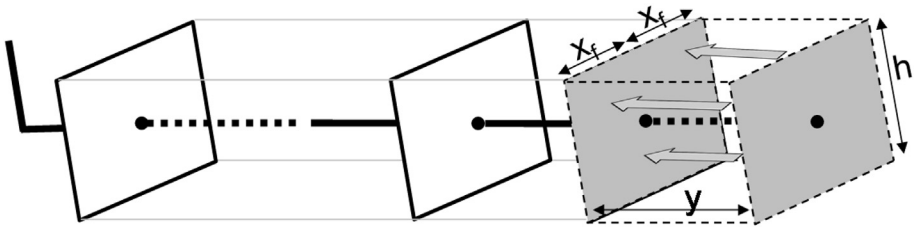

Fig. 6. A symmetrical multi-stage fractured horizontal well. The shaded area is used to effectively model the behavior of an *equivalent* 1D fracture.

Table 3
Parameters adjusted for history-matching.

		index	Parameter description	Min	Max
Initialization	**Water**	X1	Movable initial water in virgin matrix	0.2	0.4
		X2	Movable initial water in the SRV	0.4	0.7
	Rock	X3	Matrix or reservoir permeability	0.00001 md	0.001 md
		X4	SRV permeability	0.01 md	10 md
	Fluid	X11	C1	0.75	0.9
		X12	C2	0.05	0.08
		X13	C3	0.04	0.08
		X14	i-C4	0.005	0.02
		X15	n-C4	0.005	0.02
		X16	i-C5	0.002	0.01
		X17	n-C5	0.002	0.01
		X18	C6	0.002	0.01
		X19	C7+	0.015	0.06
PVT(C7+ Characterization)		X5	MW of C7+	100	140
		X6	SG of C7+	0.75	0.9
Relative Permeability (Corey's)		X7	N_w	2	4
		X8	N_{ow}	2	4
		X9	N_g	2	4
		X10	N_{og}	2	4
Fracture Permeability Reduction		X20	γ	1E-6	0.01

$$L = \frac{Q_{w_r}}{2x_f h\varphi(S_{w_{SRV}} - S_{w_{init}})} \quad (2)$$

where L is the width of the SRV. Therefore, by assuming a different initial water saturation profile for the reservoir model in each simulation run, the lateral extent of the SRV is also adjusted.

4.1.1.2. Fluid. The initial *in situ* gas condensate fluid composition was considered as an unknown parameter vector for history-matching.

4.1.2. PVT

The Peng Robinson equation-of-state (PR EOS) was selected for use in compositional simulations. The Specific Gravity (SG) and Molecular Weight (MW) of C_{7+} were considered to be unknown parameters. These two parameters are used to estimate the other related properties using some well-known correlations in commercial fluid characterization packages. Specifically, Boiling Point Temperature (Tb) was obtained from Søreide (1989), Critical Pressure (Pc), Critical Temperature (Tc), and Critical Volume (Vc) from Riazi and Daubert (1980), Acentric Factor (AC) from Edmister (1958), and Parachor values from Katz and Saltman (1939). The high uncertainty in measured properties of C_{7+} was the main reason for selecting a general correlation with some ranges of MW and SG rather than selecting all individual properties as separate history-matching parameters. This simplification can help reduce the dimensionality of the problem.

4.1.3. Relative permeability data

Corey's equation (Corey, 1954) was used to generate the 3-phase relative permeability data. The Corey exponents were used as another set of the history-matching parameters to adjust the shape of the relative permeability curves. All initial saturations and end point values were defaulted (e.g. the initial and residual saturations = 0.15) as documented in CMG-GEM™ (CMG, 2014). In other words, the endpoint saturations and the endpoint relative permeability data were fixed, and the history-matching was performed by adjusting the Corey exponents. Obviously, including these endpoint variables in the parameter spaces not only can result in different solutions but can also unnecessarily hinder the convergence due to increase of dimensionality (Keogh and Mueen, 2010). The extra parameters can be added later if the convergence allows the inclusion of extra variables or whenever some measured data became available. Nevertheless, at this stage, it is important to note that any solution to a history-matching (or optimization) problem is non-unique. The non-uniqueness in solution is an inherent characteristic of any inverse problem. However, we attempt to incorporate all available data into a unified template to reduce the uncertainty in modeling and subsequently reduce the non-uniqueness in solution.

4.1.4. Fracture permeability reduction

Rigorous modeling of geomechanics requires a coupled approach to include the stress-strain solutions into reservoir simulation (Heffer et al., 1992; Settari and Mourits, 1998). This approach, however, is computationally expensive and is not the purpose of this study. In this paper, we assumed that the proppant was mainly confined to the main fracture, whereas the fracture network within the SRV is unpropped. This in turn, results in a high fracture conductivity. To simulate the effect of geomechanics on the propped fracture, a simplified equation was used to mimic the hydraulic fracture permeability reduction as a function of pressure (Yilmaz et al., 1991; Yu and Sepehrnoori, 2014), i.e.:

$$k_f = k_i exp(\gamma(p - p_i)) \quad (3)$$

in which, "k_f" and "k_i" are the current and the original fracture permeabilities at "p" and "p_i" with p_i being the initial reservoir pressure, and "γ" is the reduction factor. Using pressure dependent permeability instead of full geomechanical was suggested

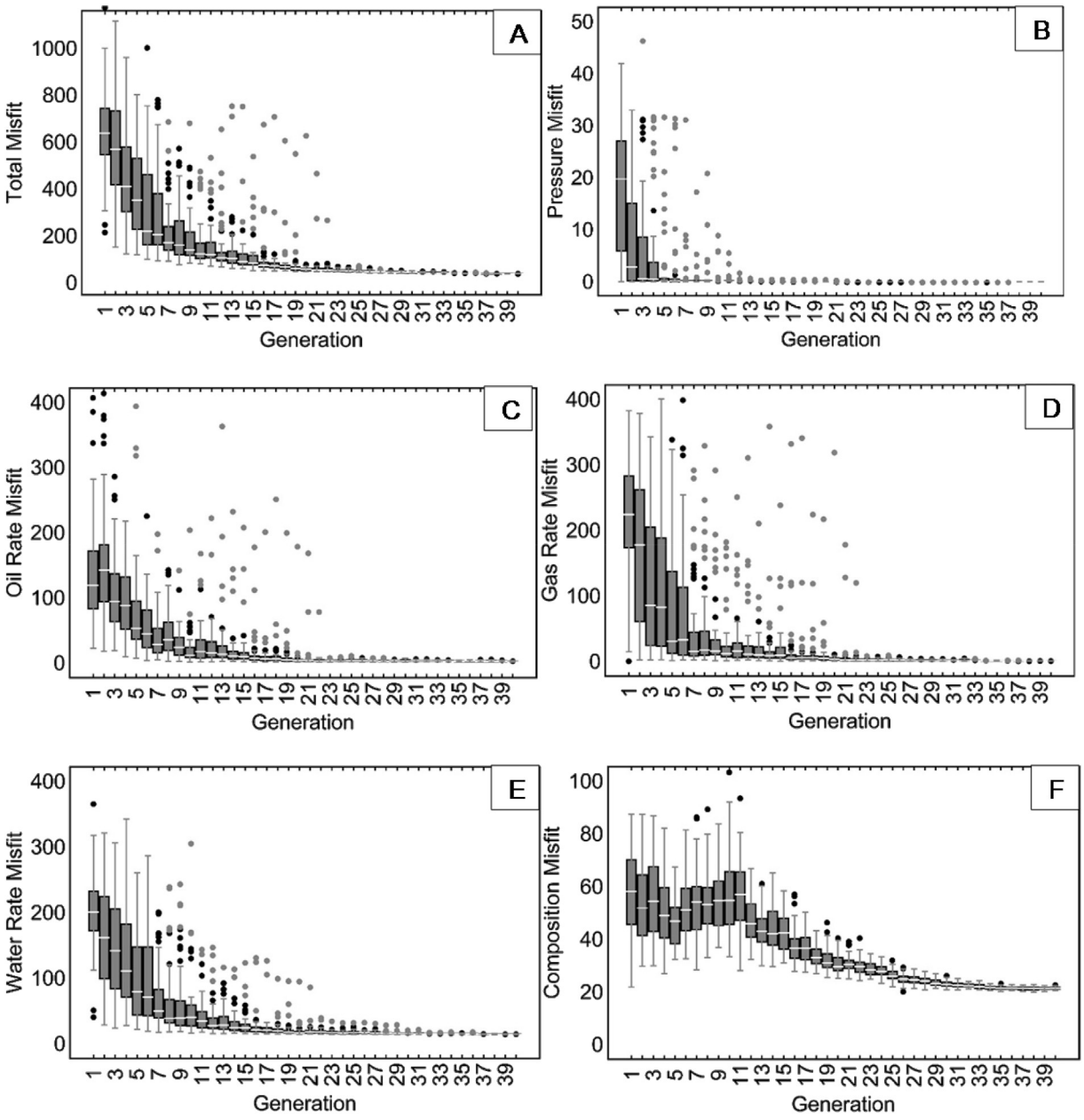

Fig. 7. Whisker-and-box-plots of misfit values as a function of generation in DE/BEST1. The total (A) and individual misfits for pressure (B), oil (C), gas (D) and water (E) rates, and total separator fluid (oil and gas) compositions (F) reduces with time (or generation). The boxes are interquartile range, the whiskers indicate the sample ranges within 3/2 interquartile from the box edges, and black and grey dots represent the outlier samples.

by Dinh et al. (2014) to be a good approximation for hard competent linear elastic rocks that are found in this field. The ranges of γ are selected to account for drastic and negligible reduction of fracture conductivity (i.e. fracture permeability times fracture width or $k_f \times w$) with production. The lowest value of 1E-6 corresponds to almost no permeability changes with pressure and a very large value of 0.01 mimics a sudden facture closure. Although in this simplified equation the change in stress is assumed to be modeled with change in pressure, which is not strictly rigorous, its simplicity and computational efficacy is advantageous. Modeling the reservoir deformation due to compaction/dilation (Batycky et al., 2007) was not considered in this modeling study.

5. Inversion

5.1. Differential evolution

The Differential Evolution with DE/BEST strategy is employed. An initial population of 50 members with random parameters (within the ranges) is generated. The scaling factor and crossover ratio are both set to 0.5. Differential Evolution runs over 40 generations with a total of 2000 simulation runs. The DE algorithm is re-run with exactly the same setting parameters and with a different random initial population to verify the existence of other possible solutions. The objective function is defined as the summation of the weighted normalized (with respect to the

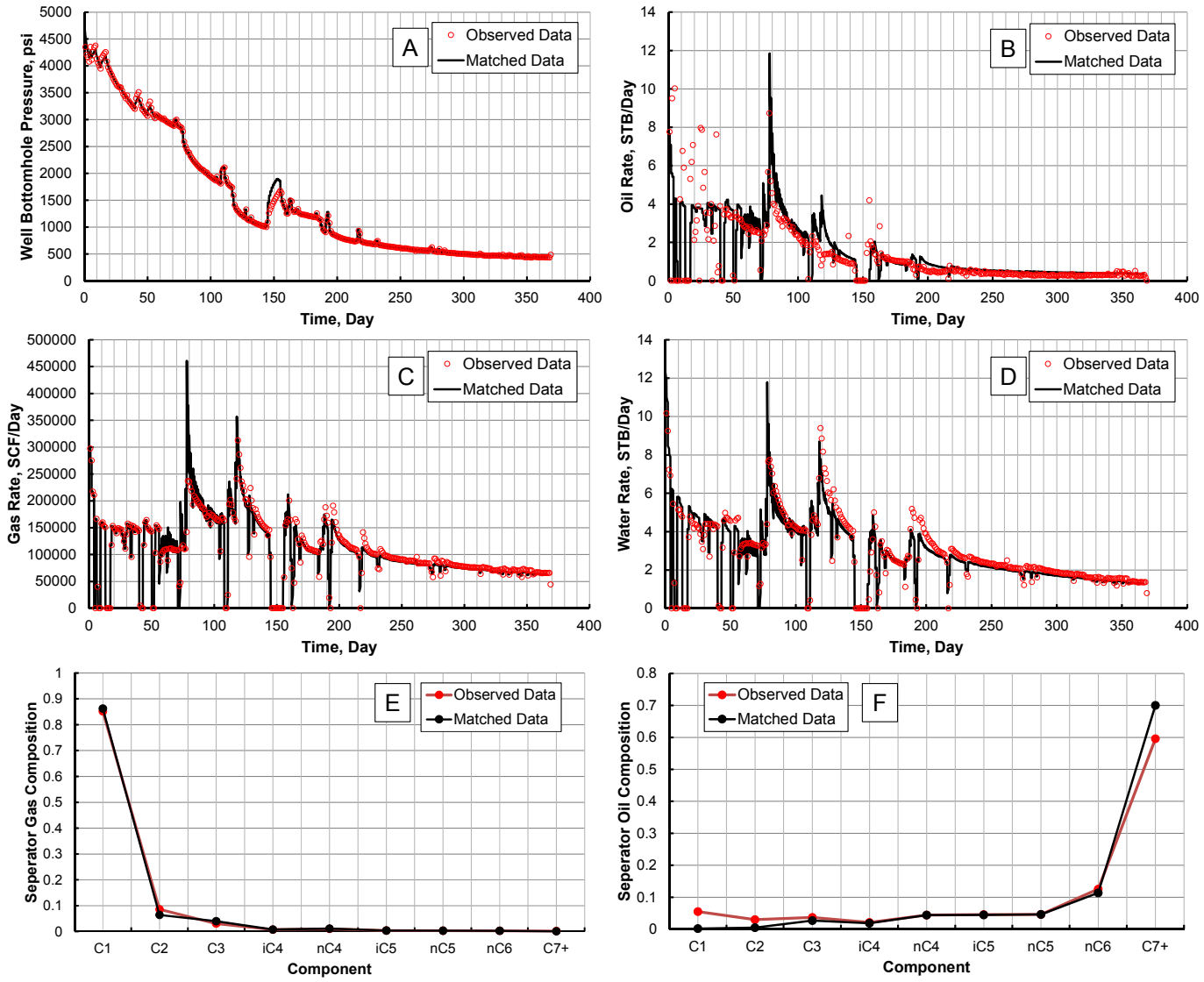

Fig. 8. The final history matching results for pressure (A), oil (B), gas (C) and water (D) and rates, and separator gas (E) and oil (F) compositions. The red curves are the measured data and the black curves are the model responses for DE1 best case. (For interpretation of the references to color in this figure legend, the reader is referred to the web version of this article.)

average value of the observed data) squared difference of the real production (subscript "obs") and simulation data (subscript "sim") (Juell and Whitson, 2013):

$$Total\ \ Missfit = \sum_{t=1}^{T}\left(\frac{q_{o\_obs}-q_{o\_sim}}{\overline{q}_{o\_obs}}\right)^2 + \sum_{t=1}^{T}\left(\frac{q_{g\_obs}-q_{g\_sim}}{\overline{q}_{g\_obs}}\right)^2 + \sum_{t=1}^{T}\left(\frac{q_{w\_obs}-q_{w\_sim}}{\overline{q}_{w\_obs}}\right)^2 + \sum_{t=1}^{T}\left(\frac{p_{obs}-p_{sim}}{\overline{p}_{obs}}\right)^2 + 10\times\sum_{c=1}^{C}\left(\frac{\delta_{obs}-\delta_{sim}}{\overline{\delta}_{obs}}\right)^2_{o,g} \quad (4)$$

where, "C" is twice the number of available components at the surface sample, "T" is the last timestep, "q" is the surface production rate, and the subscripts "o", "w", and "g" indicate oil, water and gas phases. The bar sign "‾" shows the arithmetic average value. For the first 44 days, we produce with a gas production constraint, and the total misfit includes the oil and water rate and flowing pressure misfits. For the remaining timesteps, the simulation is switched to the flowing bottomhole pressure constraint, and the total misfit is now the summation of oil, water and gas rates and composition (δ) misfits. The composition misfit is calculated at a certain timestep where the reliable measured composition is available (at day 100). The composition misfit is comprised of the total misfits of both oil and gas compositions at the separator. A weight factor of 10 has been used for the composition misfit to ensure that its value is of the same order of magnitude as the other misfit values. This factor was pre-determined before running the DE algorithm based on comparing the misfit values obtained from some initial flow simulation runs designed by a quasi-random sequence sampling experiment. The last term could also be

expanded as follows

$$\sum_{c=1}^{C}\left(\frac{\delta_{obs}-\delta_{sim}}{\overline{\delta_{obs}}}\right)_{o,g}^{2}=\left(\frac{m_{C1-obs}-m_{C1-sim}}{\overline{m_{C1-obs}}}\right)_{o}^{2}+\left(\frac{m_{C2-obs}-m_{C2-obs}}{\overline{m_{C2-obs}}}\right)_{o}^{2}+\ldots+\left(\frac{m_{C1-obs}-m_{C1-sim}}{\overline{m_{C1-obs}}}\right)_{g}^{2}+\left(\frac{m_{C2-obs}-m_{C2-obs}}{\overline{m_{C2-obs}}}\right)_{g}^{2}+\ldots \quad (5)$$

in which, "m" is the molar fraction, C_1 is Methane and C_2 is Ethane.

One problem with such a common definition of total misfit (as a weighted summation of all misfits) is that, although the total misfit may eventually converge, the process cannot guarantee the individual misfits to also converge simultaneously. However, as we will see in our results, this issue is not important for our problem as there is no strong conflict between the individual misfit values. Therefore, while the total misfit reduces, the individual misfits also reduce in later generations. Otherwise, the multi-objective optimization procedure might be an alternate choice (Coello Coello et al., 2007; Mezura-Montes et al., 2008).

5.2. Convergence

Fig. 7A through F show the whisker-and-box-plots (Weisstein, 2014) of total and individual misfits from DE progress with generation. The boxplot is a visual representation of data statistics. Each box represent $Q_1 = 25\%$ (the lower edge), $Q_2 = 50\%$ (the middle line) and $Q_3 = 75\%$ (the upper edge) quartiles. The extended whiskers represent the range within 3/2 times the interquartile range Q_3-Q_1. The black and grey dots above each box denote the outliers. The Fig. (7A through F) show that the acceptable convergences are attained for all misfits after around generation 30 (with a corresponding member or simulation case 1500). Because of the importance of oil rate matching (as it is the fluid that company starts to sell since the start of production), selection of the simulation cases with minimum total misfits were not of primary interest because it was associated with a relatively higher oil misfit. Hence, the resulting misfit data from DE were ordered based on ascending oil rate misfit, and the cases with lower global misfit were probed to check the quality of match in all individual rates and composition curves. Hence, simulation case 1761 (DE1/BEST) was selected as a case with acceptably reduced total and individual misfits for the first try of running the Differential Evolution algorithm (DE1). Table 4 summarizes two sets of parameter vectors as outcomes of performing the optimization algorithm from two distinct Differential Evolution trials with the same set–up parameters. One interesting point is that the geomechanical effect (X20) appears to be minimal particularly for the second Differential Evolution run (DE2). Almost similar values for water saturations (X1 and X2) were obtained in both runs. DE2 was only performed to show the non-uniqueness of the solution where different random initial population can lead to different solution vectors. The combination of both DE resultant samples can provide invaluable information to explore and analyze the performance of our model in terms of parameter interactions and their global effects on the production data.

Fig. 8A through F, represent the history-match results of DE1's best solution. Fig. 8A through F, represent the history-match results of DE1's best solution. As Fig. 8 shows, a good match has been obtained which can approximately represent the available data. There is an apparent early mismatch in the oil production data which could not be furthered improved in this study. However, this is likely due to the existence of high uncertainty in the noisy measurement data in the early times. The corresponding solution of DE2 (i.e. simulation case 1289) can produce the same quality of matches of the data as DE1, but is not shown here.

Table 4
The best case solution vectors obtained from two separate runs of differential evolution DE/BEST with different initial population.

Parameters	DE1/BEST (simulation 1761)	DE2/BEST (simulation 1289)
X1	0.287	0.351
X2	0.437	0.498
X3	0.00022	0.00040
X4	4.434	0.562
X5	109.299	129.530
X6	0.848	0.788
X7	2.003	3.884
X8	3.114	3.227
X9	3.876	3.995
X10	2.000	3.760
X11	0.881	0.895
X12	0.066	0.067
X13	0.043	0.043
X14	0.009	0.008
X15	0.013	0.014
X16	0.005	0.005
X17	0.004	0.004
X18	0.005	0.004
X19	0.021	0.016
X20	7.95E-04	2.00E-06
Total Misfit	45.60	54.58

The estimated fluid composition for DE1's matched case (DE1/BEST) corresponds to a lean gas condensate fluid with a maximum oil saturation of 1.5% from the CCE test and has a dew point pressure of 2708 psi at reservoir temperature of 162 °F. On the other hand, the saturation pressure of DE2/BEST is 2585.5 psi with a maximum liquid saturation of 1.3% from CCE test.

6. Sensitivity analysis

The purpose of the sensitivity analysis is to investigate which parameters cause more output uncertainty and to quantify the confidence on the solution parameters. Differential Evolution creates a pool of samples, which have adapted or evolved from an initial random generation towards some solutions with minimal misfits. Using the DE/BEST scheme conveys that the final accepted solution was mainly inherited from a best member somewhere in the generation and therefore, the process doesn't guarantee to find all available solutions. To have a better understanding of the model input–output relationships, global sensitivity methods can be used to provide a wider perspective on the performance and sensitivity of the misfits to the model parameters within the entire range of the allowable inputs (Tong and Graziani, 2008). Total sensitivity indices can take into account the interactions between parameters in the sensitivity calculations. In this study, we use the total order Sobol' indices (S_{Ti}) that are based on the decomposition of variance and indicate the contribution of each parameter (X) to the total output (Y) variance, where parameter interactions are also included (Sobol', 1967; Saltelli, 2002; Schwieger, 2006). This can be formulated as $S_{Ti} = \mathbf{E}(\mathbf{V}(Y|X_{\sim i}))/\mathbf{V}(Y)$, where the subscript ~ i represents all input variables except X_i, and **E** and **V** are the expected value and the variance. The calculation methods are based on partial variance

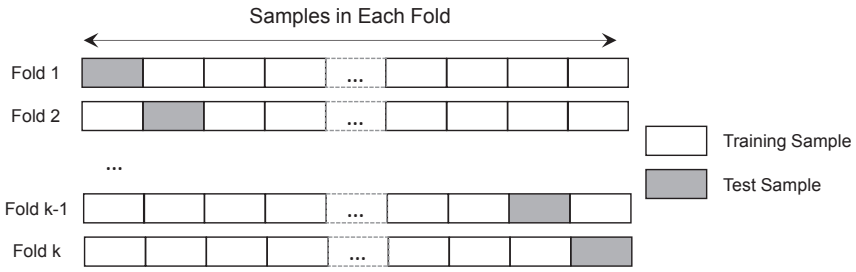

Fig. 9. The k-fold cross validation. The proxy model is constructed for each fold (or subset) from the training samples and is used to predict the output of the test sample.

Table 5
The training (fitting) and cross validation errors associated with MARS to model oil and gas rates, and composition misfits.

Error	Oil misfit		Gas misfit		Composition misfit	
	Training	CV	Training	CV	Training	CV
Average error	0.126	0.169	0.038	0.050	0.000	0.000
RMS error	0.890	1.147	0.593	0.674	0.018	0.020
MAX error	8.335	13.920	10.010	14.240	0.117	0.119
R-square	0.989		0.998		0.998	

the objective function misfit values) in a faster way. Finding a validated response surface is not a simple task and requires considerable effort and time to find the reliable settings. However, our numerical experiences in production and well test history-matching and uncertainty quantification demonstrated that the Multivariate Adaptive Regression Splines or MARS (Friedman, 1991) can be a rather good response surface for our application. The MARS model is a nonparametric approach to model the nonlinearity and interactions between the variables in high dimensional spaces (Friedman, 1991) without considering any assumption for the

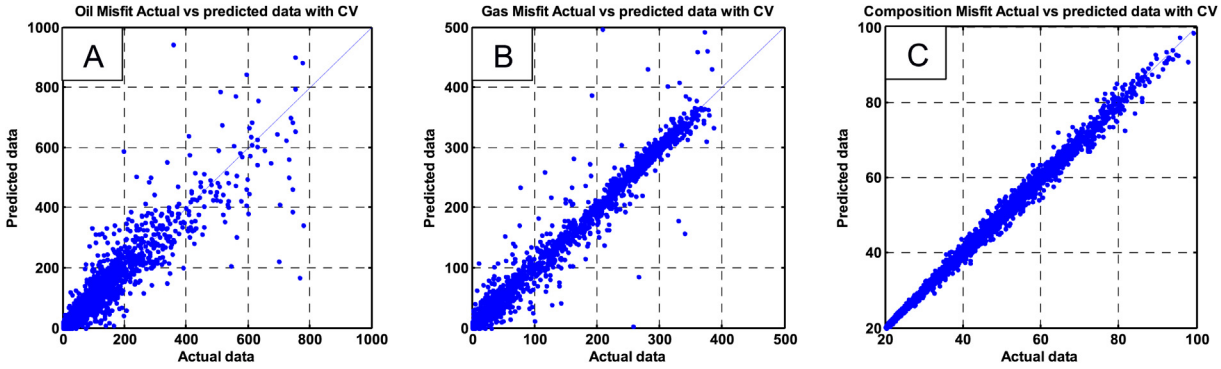

Fig. 10. The training (fitting) and cross validation errors associated with MARS to model oil and gas rates, and composition misfits.

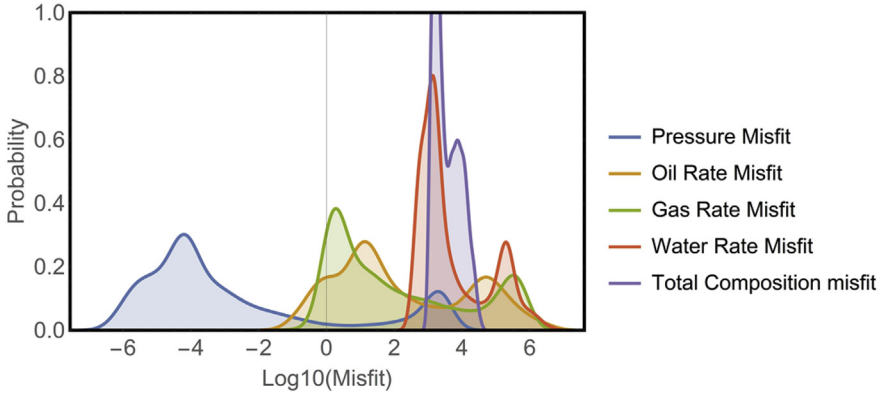

Fig. 11. The smooth histogram of individual log misfits. The total composition misfit has a narrower variation range.

integral calculations by numerical methods (Tong, 2013). The sensitivity indices require rigorous sampling and function evaluations, which make the process computationally costly. Therefore, the response surface models or RSM's (also known as Meta models or proxies) are favorable to approximate the response function (i.e. model input–output functional relationships. MARS has proven to be a robust response surface model in various engineering applications (Leathwick et al., 2005; Balshi et al., 2009; Zhan et al., 2013; Hamdi et al., 2014). MARS divides the input parameter space into some sub-regions using some knot points and uses different

regression equations within each subset to model the input–output relationships. The MARS regression function is a linear combination of many basis functions, and each basis function is a truncated power spline and includes a degree of interactions between the parameters (Sakamoto, 2007). The detail of MARS regression function is documented in Friedman (1991).

The MARS model is constructed based on the available pool of data created from Differential Evolution. However, as mentioned earlier for adaptive sampling, as in DE, it may not adequately cover the parameter space, and the samples might only represent a portion of the space with a higher density in the solution areas. An additional space-filling sample design can improve the quality of the RSM. A quasi-random sequence sampling method has shown to be an appropriate design for the global sensitivity analysis particularly, when the numerical integration should be evaluated (Sobol', 1967). Hence, in this study, an additional 1000 samples from our 20-dimensional parameter space are generated and the outputs (or misfits) are evaluated directly from the simulation runs. These samples are added to the already generated pool of samples from two separate Differential Evolution runs with 4000 samples. Still, the constructed MARS model from these 5000 samples should be validated to ensure the productivity of the RSM. K-fold cross validation is a common statistical approach which splits the training samples into k subsets of equal size (Geisser, 1993). For each subset, one sample is left out (i.e. the test sample), and the model is constructed for the remaining samples to calculate the error associated with the prediction of test sample output (Fig. 9). This process is a time-consuming and must be repeated for all k folds.

In this study, we use the number of subsets k = 500, which roughly takes 30 h to complete for each misfit (i.e. composition, oil, water and gas misfits). For the purpose of this study, a MARS model with 300 basis function and 20 interaction levels between the input variables provided a reasonable fit to the training data to reproduce the model output (i.e. the misfits associated with hydrocarbon rates and total separator compositions). Many other types of response surfaces such as k-nearest neighbors (Kuhn and Johnson, 2013), radial basis functions (Kuhn and Johnson, 2013) and kriging response surfaces (Rasmussen and Williams, 2005) were also tried. However, only the MARS model could reproduce the lower errors within a considerably smaller time frame. Table 5 summarizes the quality of the MARS model in terms of training (fitting) and cross validation errors. The prediction ability of this MARS model from 500-fold cross validation is also shown in Fig. 10. Clearly, the quality of modeling for total separator composition is better than the ones for the oil and gas rates misfits as the data are more aligned on the 45° diagonal line (i.e. MARS model could better predict the hold out samples). This might reflect the different nature of the misfit values. The misfit data for the rates are averaged over all timesteps, which showed higher variation ranges than the composition misfit that is averaged over the components in a single timestep (Fig. 11). Therefore, the rate misfits can carry a higher variation level and therefore are more difficult to represent with a proxy model. Considering the computational time, here we only consider the sensitivity analysis for the hydrocarbon rates, and total composition misfits. Obviously, the same set of analysis can also be performed on the water rate misfit.

The total order Sobol' indices are quantified by drawing and evaluating 100,000 sample points from the validated MARS RSM by assuming the uniform distribution over the input parameters. The calculated Sobol' indices are averaged over 500 bootstrap runs. This process takes around 48 h to complete for each misfit. Fig. 12 shows the calculated average bootstrap Sobol' indices for total composition, oil, gas and water misfits. The pads with green circles on each bar indicate the standard deviations associated with sensitivity indices over 500 repeated trails. A quick look at the Fig. (12A through C) reveals that as the quality of RSM for predicting the total composition is better, the standard deviations associated with total sensitivity indices are lower. The sensitivity indices are used to rank the important parameters that convey greater information for the model output. Moreover, they can show the uncertainty in each parameter. In this sense, the parameters with lower total sensitivity indices have higher uncertainties. In other words, because the output is less sensitive to an input parameter, the estimated parameter conveys less information about the output. Fig. 12A shows that the fracture permeability reduction factor or geomechanical effects (X20), reservoir permeability (X3), *in situ* SG of C_{7+}(X6), and movable initial water saturations in the SRV and

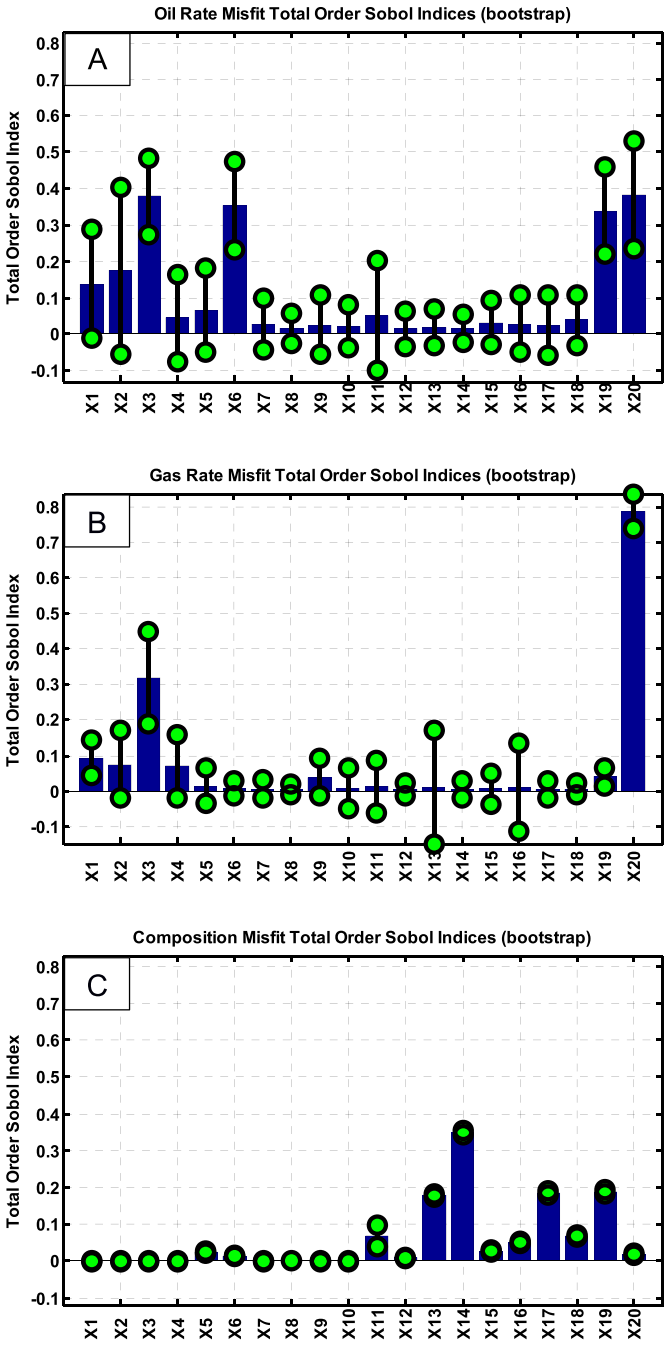

Fig. 12. Total order Sobol' sensitivity indices used to rank the importance of the input descriptive model parameters for oil (A), gas (B) and total composition (C) misfits.

reservoir rock (X2 and X1) have higher impacts on the oil rate misfits. Whereas, geomechanical effects (X20) and reservoir permeability (X3) have dominant impacts on the gas misfits (Fig. 12B). Sobol' indices for the total composition misfit reveal that the *in situ* compositions of i-C4 (X14), C3 (X13), n-C5 (X17) and C_{7+} (X19) compete for altering the total composition output (Fig. 12C).

7. Conclusions

In this work, we successfully implemented the Differential Evolution (DE) algorithm to history-match fluid production and separator composition data for a liquid-rich, tight gas condensate well in the Montney Formation. The results help characterize a consistent 1D linear model, including a hydraulic fracture with a surrounding SRV, and to construct a reliable *in situ* gas condensate fluid model. The history-matched results can satisfactorily reproduce the water and hydrocarbon surface flow rates, flowing bottomhole pressure, and separator fluid compositions. The surface samples were very important to reduce the uncertainty in the number of components and their variation ranges in the equation of state (PR EOS) used to model fluid. The best solution obtained from the DE optimization algorithm led to a lean gas condensate fluid with around 1.5% of liquid dropout from the CCE test.

One advantage of using the DE algorithm is that it provides a pool of samples, and a set of solutions, that can be further used to statistically evaluate the performance of our model in terms of global sensitivity analysis. The total order Sobol' indices were calculated to rank the importance of parameters. For example, the fracture permeability reduction factor with pressure and the matrix permeability were found to have the largest impact on the uncertainty of both hydrocarbon rates, while they have minimal effects on the total separator composition. The permeability of the SRV, the initial water distributions, and SG of C_{7+} were the other important factors controlling oil rate.

It is important to note that the DE results still remain non-unique solutions to a nonlinear inverse problem. Nevertheless, the importance of this work is that it describes a workflow that integrates the available data and enables the uncertainty in the fluid behavior and reservoir model to be addressed in an efficient way. The approach we followed in this paper was to downgrade the production data analysis of a multi-physics problem by employing some simplifying assumptions, such as: 1) using an equivalent 1D linear model 2) a simple fracture permeability reduction model with pressure rather than a comprehensive geomechanical model, and 3) a stepwise movable initial water saturation profile, and 4) ignoring sorption effects and non-Darcy flow. However, once again, this does not affect the generality of the approach and more details can be added to the system depending on the purpose of the study, and the level of complexity required.

Acknowledgments

Hamidreza Hamdi would like to thank the Interactive Reservoir Modeling, Visualization and Analytics Research Group at the Department of Computer Science at the University of Calgary for supporting his postdoctoral fellowship. The authors would like to thank the sponsors of Tight Oil Consortium for funding this project. The authors acknowledge Dr. Curtis Whiston for discussion and helpful comments on the manuscript. Chris Clarkson would like to acknowledge Encana, Shell and Alberta Innovates Technology Futures for support of his Chair in Unconventional Gas and Light Oil Research in the Department of Geoscience, University of Calgary.

References

Adams, C., 2013. The status of drilling and production in BC's shale gas plays. 5th Northeast B.C. Natural Gas Summit, Vancouver, BC, Canada. September 23 – 24.
Al Ghamdi, B.N., Ayala, L.F., 2010. Analysis of capillary pressure and relative permeability effects on the productivity of naturally fractured gas-condensate reservoirs. Paper SPE 136943-MS, Presented at the SPE/DGS Saudi Arabia Section Technical Symposium and Exhibition, Al-Khobar, Saudi Arabia 4-7 April.
Albright, J.N., Pearson, C.F., 1982. Acoustic emissions as a tool for hydraulic fracture location: experience at the Fenton Hill hot dry rock site. SPE J. 22 (4), 523–530. Pap. SPE 9509-PA.
Atkinson, K.E., 1978. An Introduction to Numerical Analysis. Wiley.
Awotunde, A.A., Mutasiem, M.A., 2014. Efficient drilling time optimization with differential evolution. Presented at the SPE Nigeria Annual International Conference and Exhibition, Lagos, Nigeria 5–7 August.
Balshi, M.S., McGuire, A.D., Duffy, P., Flannigan, M., Walsh, J., Melillo, J., 2009. Assessing the response of area burned to changing climate in western boreal North America using a multivariate adaptive regression splines (MARS) approach. Glob. Change Biol. 15 (3), 578–600.
Bard, Y., 1974. Nonlinear Parameter Estimation. Academic Press, NY, p. 341.
Barree, R.D., 2013. Overview of current DFIT analysis methodology (SPE). http://eo2.commpartners.com/users/spe/session.php?id=10329.
Batycky, R.P., Thiele, M.R., Coats, K.H., Grindheim, A., Ponting, D., Settari, T., Wallis, J., Watts, J.W., Whitson, C.H., 2007. Geomechanics in reservoir simulation. In: Lake, L.W., Holstein, E.D. (Eds.), Petroleum Engineering Handbook: Volume V – Reservoir Engineering and Petrophysics, vol. V. Society of Petroleum Engineers, Richardson, Texas, USA.
Bazan, L.W., Larkin, S.D., Lattibeaudiere, M.G., Palisch, T.T., 2010. Improving production in the Eagle Ford shale with fracture modeling, increased fracture conductivity, and optimized stage and cluster spacing along the horizontal wellbore. Paper SPE 138425–MS, Presented at the Tight Gas Completions Conference, San Antonio, Texas, USA 2-3 November.
Beggs, D.H., Brill, J.P., 1973. A study of two-phase flow in inclined pipes. J. Pet. Technol. 25 (05), 607–617. Pap. SPE 4007-PA.
Behmanesh, H., Hamdi, H., Clarkson, C.R., 2015. Production data analysis of tight gas condensate reservoirs. J. Nat. Gas Sci. Eng. 22 (0), 22–34.
Behmanesh, H., Hamdi, H., Heidari Sureshjani, M., Clarkson, C.R., 2014. Production data analysis of overpressured liquid-rich shale reservoirs: effect of degree of undersaturation. Paper SPE 168980–MS, Presented at the SPE Unconventional Resources Conference, the Woodlands, Texas, USA 2014/4/1/.
Bhattacharya, S., Nikolaou, M., 2013. Analysis of production history for unconventional gas reservoirs with statistical methods. SPE J. 18 (5), 879–896.
Board, N.E., 2013. The Ultimate Potential for Unconventional Petroleum from the Montney Formation of British Columbia and Alberta – Energy Briefing Note, vol. 2013. National Energy Board. http://www.neb-one.gc.ca/nrg/sttstc/ntrlgs/rprt/ltmtptntlmntnyfrmtn2013/ltmtptntlmntnyfrmtn2013-eng.html.
Cipolla, C.L., Lolon, E., Erdle, J., Tathed, V.S., 2009. Modeling well performance in Shale-gas reservoirs. Paper SPE 125532-MS Presented at the SPE/EAGE Reservoir Characterization and Simulation Conference, Abu Dhabi, UAE, 19–21 October.
Cipolla, C.L., Lolon, E.P., Erdle, J.C., Rubin, B., 2010. Reservoir modeling in Shale-gas reservoirs. SPE Reserv. Eval. Eng. 13 (14), 638–653. Pap. SPE 125530.
CMG, 2014. GEM User's Guide: Advanced Compositional and Unconventional Reservoir Simulator Version 2014.
Coello Coello, C., Lamont, G., Van Veldhuizen, D., 2007. Evolutionary Algorithms for Solving Multi-objective Problems (Genetic and Evolutionary Computation). Springer.
Corey, A.T., 1954. The interrelation between gas and oil relative permeabilities. Prod. Mon. 19, 38–41.
Decker, J., Mauldon, M., 2006. Determining size and shape of fractures from trace data using a differential evolution algorithm. Paper SPE ARMA-06-969, Presented at the Golden Rocks 2006, the 41st U.S. Symposium on Rock Mechanics (USRMS), Golden, Colorado, USA, 17-21 June.
Detring, J., Williams-Stroud, S., 2013. The use of microseismicity to understand subsurface-fracture systems and to increase the effectiveness of completions: eagle Ford shale, Texas. SPE J. 13 (4), 1–5. Pap. SPE 162845-PA.
Dinh, V.P., Gouge, B.A., White, A.J., 2014. Estimating long term well performance in the montney shale gas reservoir. Paper SPE 169843-MS, Presented at the SPE Hydrocarbon Economics and Evaluation Symposium, Houston, Texas, USA, 19-20 May.
Edmister, W.C., 1958. Applied hydrocarbon thermodynamic, part 4: compressibility factors and equations of state. Pet. Refin. 37, 173–179.
Enyioha, C., Ertekin, T., 2014. Advanced well structures: an artificial intelligence approach to field deployment and performance prediction. Paper SPE 167870–MS, Presented at the SPE Intelligent Energy Conference & Exhibition, Utrecht, The Netherlands, 1-3 April.
Epitropakis, M.G., Plagianakos, V.P., Vrahatis, M.N., 2008. Balancing the exploration and exploitation capabilities of the differential evolution algorithm, evolutionary computation, 2008. CEC 2008. (IEEE World Congress on Computational Intelligence). IEEE Congress on, pp. 2686–2693, 1-6 June 2008.
Fan, L., Martin, R.B., Thompson, J.W., Atwood, K., Robinson, J.R., Lindsay, G.J., 2011. An integrated approach for understanding oil and gas reserves potential in Eagle Ford shale formation. Paper SPE 148751-MS, Presented at the Canadian Unconventional Resources Conference, Alberta, Canada 15-17 November.

Fanchi, J.R., 2000. Integrated Flow Modeling. Elsevier, p. 304.

Fanchi, J.R., 2002. Shared Earth Modeling. Butterworth-Heinemann.

Fisher, M.K., Heinze, J.R., Harris, C.D., Davidson, B.M., Wright, C.A., Dunn, K.P., 2004. Optimizing horizontal completion techniques in the Barnett shale using microseismic fracture mapping. Paper SPE 90051-MS, Presented at the SPE Annual Technical Conference and Exhibition, Houston, Texas, USA, 26-29 September.

Forchheimer, P., 1901. Wasserbewegung durch boden. Z. Des. Vereines Dtsch. Ingenieure 45, 339–355.

Friedman, J.H., 1991. Multivariate adaptive regression splines. Ann. Stat. 19 (1), 1–67.

Geisser, S., 1993. Predictive Inference. Taylor & Francis.

Ghods, P., Zhang, D., 2010. Ensemble based characterization and history matching of naturally fractured tight/shale gas reservoirs. Paper SPE 133606-MS, Presented at the SPE Western Regional Meeting, Anaheim, California, USA 27-29 May.

Gilman, J.R., Ozgen, C., 2013. Reservoir Simulation: History Matching and Forecasting: Richardson. Society of Petroleum Engineers, TX.

Gorucu, S.E., Ertekin, T., 2011. Optimization of the design of transverse hydraulic fractures in horizontal wells placed in dual porosity tight gas reservoirs. Paper SPE 142040–MS, Presented at the SPE Middle East Unconventional Gas Conference and Exhibition, Muscat, Oman, 31 January-2 February.

Hajizadeh, Y., Christie, M.A., Demyanov, V., 2009a. Ant colony optimization for history matching. Paper SPE SPE-121193-MS, Presented at the EUROPEC/EAGE Conference and Exhibition, Amsterdam, The Netherlands, 8-11 June 2009.

Hajizadeh, Y., Christie, M.A., Demyanov, V., 2009b. Application of differential evolution as a new method for automatic history matching. Paper SPE SPE-127251-MS, Presented at the Kuwait International Petroleum Conference and Exhibition, Kuwait City, Kuwait, 14-16 December.

Hamdi, H., Hajizadeh, Y., Azimi, J., Sousa, M.C., 2014. Sequential Bayesian optimization coupled with differential evolution for geological well testing. Presented at the 76th EAGE Conference and Exhibition 2014 Amsterdam, the Netherlands, 16–19 June 2014.

Hamdi, H., Hajizadeh, Y., Costa Sousa, M., 2015. Population Based Sampling Methods for Geological Well Testingadate (*in press* with Computational Geoscience journal).

Heffer, K.J., Last, N.C., Koutsabeloulis, N.C., Chan, H.C.M., Gutierrez, M., Makurat, A., 1992. The influence of natural fractures, faults and earth stresses on reservoir performance – geomechanical analysis by numerical modelling. In: Aasen, J.O., Berg, E., Buller, A.T., Hjelmeland, O., Holt, R.M., Kleppe, J., Torsæter, O. (Eds.), North Sea Oil and Gas Reservoirs III: Trondheim. Kluwer Academic Publishers, Norway, pp. 201–211.

Houzé, O., Viturat, D., Fjaere, O.S., Trin, S., Allain, O., Tauzin, E., 2011. Dynamic Data Analysis: The Theory and Practice of Pressure Transient, Production Analysis, Well Performance Analysis, Production Logging and the use of Permanent Downhole Gauge Data (Ebook). KAPPA, p. 505.

Jolliffe, I.T., 2002. Principal Component Analysis, second ed. Springer-Verlag New York, Inc, New York, p. 488.

Jones, D., 2001. A taxonomy of global optimization methods based on response surfaces. J. Glob. Optim. 21 (4), 345–383.

Jones, D.R., Schonlau, M., Welch, W.J., 1998. Efficient global optimization of expensive black-box functions. J. Glob. Optim. 13 (4), 455–492.

Juell, A.O., Whitson, C.H., 2013. Optimized well modeling of liquid-rich shale reservoirs. Paper SPE 166380-MS, Presented at the SPE Annual Technical Conference and Exhibition, New Orleans, Louisiana, USA 30 September-2 October.

Jurus, W.J., Whitson, C.H., Golan, M., 2013. Modeling water flow in hydraulically-fractured shale wells. Paper SPE 166439-MS, Presented at the SPE Annual Technical Conference and Exhibition, New Orleans, Louisiana, USA 30 September-2 October.

Kalantari Dahaghi, A., Esmaili, S., Mohaghegh, S.D., 2012. Fast track analysis of shale numerical models. Paper SPE 162699-MS, Presented at the SPE Canadian Unconventional Resources Conference, Calgary, Alberta, Canada, 30 October-1 November.

Katz, D.L., Saltman, W., 1939. Surface tension of hydrocarbons. Indus. Eng. Chem. 31 (1), 91–94.

Keogh, E., Mueen, A., 2010. Curse of dimensionality. In: Sammut, C., Webb, G. (Eds.), Encyclopedia of Machine Learning. Springer, US, pp. 257–258.

Klinkenberg, L.J., 1941. The permeability of porous media to liquids and gases. Paper SPE API-41-200, Presented at the Drilling and Production Practice, New York, USA, 1941/1/1/.

Kuhn, M., Johnson, K., 2013. Applied Predictive Modeling. Springer, p. 613.

Langmuir, I., 1916. THE constitution and fundamental properties of solids and liquids. Part I. Solids. J. Am. Chem. Soc. 38 (11), 2221–2295.

Leathwick, J.R., Rowe, D., Richardson, J., Elith, J., Hastie, T., 2005. Using multivariate adaptive regression splines to predict the distributions of New Zealand's freshwater diadromous fish. Freshw. Biol. 50 (12), 2034–2052.

Lee, W.J., Sidle, R.E., 2010. Gas reserves estimation in resource plays. Paper SPE 130102-MS, Presented at the SPE Unconventional Gas Conference, Pittsburgh, Pennsylvania, USA 23-25 February.

Mattar, L., Anderson, D., Thompson, J., Nobakht, M., Liang, P., Morad, K., 2011. Unconventional Gas-Meaning of Permeability, Fekete's Technical Newsletter, pp. 2–3. Fekete. http://www.fekete.com/technical-resources/Pages/Technical-Newsletters.aspx.

Maxwell, S.C., Urbancic, T.I., Steinsberger, N., Zinno, R., 2002. Microseismic imaging of hydraulic fracture complexity in the Barnett shale. Paper SPE 77440-MS, Presented at the SPE Annual Technical Conference and Exhibition, San Antonio, Texas, USA, 29 September-2 October.

Maxwell, S.C., Waltman, C., Warpinski, N.R., Mayerhofer, M.J., Boroumand, N., 2009. Imaging Seismic deformation induced by hydraulic fracture complexity. SPE Reserv. Eval. Eng. 12 (1), 48–52. Pap. SPE 102801-PA.

Mayerhofer, M.J., Lolon, E., Warpinski, N.R., Cipolla, C.L., Walser, D.W., Rightmire, C.M., 2010. What is stimulated reservoir volume? SPE Prod. 25 (1), 89–98. Operations, Pap. SPE 119890-PA.

Mayerhofer, M.J., Lolon, E.P., Youngblood, J.E., Heinze, J.R., 2006. Integration of microseismic-fracture-mapping results with numerical fracture network production modeling in the Barnett shale. Paper SPE 102103-MS, Presented at the SPE Annual Technical Conference and Exhibition, San Antonio, Texas, USA 24-27 September.

Mezura-Montes, E., Reyes-Sierra, M., Coello, C.C., 2008. Multi-objective optimization using differential evolution: a survey of the state-of-the-art. In: Chakraborty, U. (Ed.), Advances in Differential Evolution, Studies in Computational Intelligence, vol. 143. Springer, Berlin Heidelberg, pp. 173–196.

Mirzabozorg, A., Nghiem, L., Yang, C., Chen, Z., 2013. Differential evolution for assisted history matching process: SAGD case study. Paper SPE 165491–MS, Presented at the SPE Heavy Oil Conference, Calgary, Alberta, Canada, 11-13 June.

Mitchell, M., 1998. An Introduction to Genetic Algorithms. MIT Press.

Nejadi, S., Leung, J.Y.W., Trivedi, J.J., Virues, C.J.J., 2014. Integrated Characterization of Hydraulically Fractured Shale Gas Reservoirs Production History Matching, Presented at the SPE/CSUR Unconventional Resources Conference. Alberta, Canada, 30 September–2 October, Calgary.

Nobakht, M., Clarkson, C.R., 2011. Analysis of production data in shale gas reservoirs: rigorous corrections for fluid and flow properties. Paper SPE 149404, Presented at the SPE Eastern Regional Meeting, Columbus, Ohio, USA, 17–19 August.

Nobakht, M., Clarkson, C.R., 2012. A new analytical method for analyzing linear flow in tight/Shale gas reservoirs: constant-flowing-pressure boundary condition. SPE Reserv. Eval. Eng. 15 (3), 370–384. Pap. SPE 143989-PA.

Nobakht, M., Mattar, L., 2012. Analyzing production data from unconventional gas reservoirs with linear flow and apparent skin. J. Can. Pet. Technol. 51 (1), 52–59. Pap. SPE 137454-PA.

Orangi, A., Nagarajan, N.R., Honarpour, M.M., Rosenzweig, J.J., 2011. Unconventional shale oil and gas-condensate reservoir production, impact of rock, fluid, and hydraulic fractures. Paper SPE 140536–MS, Presented at the SPE Hydraulic Fracturing Technology Conference, the Woodlands, Texas, USA, SPE Hydraulic Fracturing Technology Conference.

Palacio, J.C., Blasingame, T.A., 1993. Decline-curve analysis with type curves – analysis of gas well production data. Paper SPE 25909-MS, Presented at the Low Permeability Reservoirs Symposium, Denver, Colorado, USA, 26-28 April.

Poli, R., Kennedy, J., Blackwell, T., 2007. Particle swarm optimization. Swarm Intell. 1 (1), 33–57.

Price, K., Storn, R.M., Lampinen, J., 2005. Differential Evolution: a Practical Approach to Global Optimization. Springer, Germany, p. 538.

Rasmussen, C.E., Williams, C.K.I., 2005. Gaussian Processes for Machine Learning (Adaptive Computation and Machine Learning). The MIT Press.

Riazi, M.R., Daubert, T.E., 1980. Simplify Property Predictions: Hydrocarbon Processing, pp. 115–116.

Rokosh, C.D., Lyster, S., Anderson, S.D.A., Beaton, A.P., Berhane, H., Brazzoni, T., Chen, D., Cheng, Y., Mack, T., Pana, C., Pawlowicz, J.G., 2012. Summary of Alberta's Shale- and Siltstone-hosted Hydrocarbons, p. 31.

Sakamoto, W., 2007. MARS: selecting basis functions and knots with an empirical Bayes method. Comput. Stat. 22 (4), 583–597.

Saltelli, A., 2002. Sensitivity analysis for importance assessment. Risk Anal. 22 (3), 579–590.

Schwieger, V., 2006. Sensitivity analysis as a general tool for model optimisation – examples for trajectory estimation. J. Appl. Geod. 1 (1), 27–34.

Settari, A., Mourits, F.M., 1998. A coupled reservoir and geomechanical simulation system. SPE J. 3 (3), 219–226. Pap. SPE 50939-PA.

Simon, D., 2013. Evolutionary Optimization Algorithms. Wiley.

Sobol', I.M., 1967. On the distribution of points in a cube and the approximate evaluation of integrals. USSR Comput. Math. Math. Phys. 7 (4), 86–112.

Søreide, I., 1989. Improved Phase Behavior Predictions of Petroleum Reservoir Fluids from a Cubic Equation of State. Norwegian Inst. of Technology, Trondheim, Norway. Doctor of Engineering thesis.

Stalgorova, E., Mattar, L., 2012a. Analytical model for history matching and forecasting production in multifrac composite systems. Paper SPE 162516-MS, Presented at the 2012 SPE Canadian Unconventional Resources Conference, Calgary, Alberta, 30 October-1 November.

Stalgorova, E., Mattar, L., 2012b. Practical analytical model to simulate production of horizontal Wells with branch fractures. Paper SPE 162515-MS, Presented at the 2012 SPE Canadian Unconventional Resources Conference, Calgary, Alberta, Canada 30 October-1 November.

Storn, R., Price, K., 1995. Differential Evolution- a Simple and Efficient Adaptive Scheme for Global Optimization over Continuous Spaces. Technical Report TR-95-012: Berkeley.

Tarantola, A., 2005. Inverse Problem Theory and Methods for Model Parameter Estimation. Society for Industrial and Applied Mathematics, p. 342.

Tong, C., 2013. PSUADE: Livermore, CA, Center for Applied Scientific Computing Lawrence Livermore National Laboratory.

Tong, C., Graziani, F., 2008. A practical global sensitivity analysis methodology for multi-physics applications. In: Graziani, F. (Ed.), Computational Methods in Transport: Verification and Validation, Lecture Notes in Computational Science and Engineering, vol. 62. Springer Berlin Heidelberg, pp. 277–299.

Warpinski, N.R., Wolhart, S.L., Wright, C.A., 2004. Analysis and prediction of microseismicity induced by hydraulic fracturing. SPE J. 9 (01), 24–33. Pap. SPE 87673-PA.
Weisstein, E.W., 2014. Box-and-Whisker Plot. from MathWorld–a Wolfram Web Resource. http://mathworld.wolfram.com/Box-and-WhiskerPlot.html.
Yilmaz, O., Nur, A., Nolen-Hoeksema, R., 1991. Pore Pressure Profiles in Fractured and Compliant Rooks. Society of Petroleum Engineers.
Yin, J., Xie, J., Datta-Gupta, A., Hill, A.D., 2011. Improved characterization and performance assessment of shale gas wells by integrating stimulated reservoir volume and production data. Paper SPE 148969-MS, Presented at the SPE Eastern Regional Meeting, Columbus, Ohio, USA, 17-19 August.
Yu, W., Sepehrnoori, K., 2014. Simulation of gas desorption and geomechanics effects for unconventional gas reservoirs. Fuel 116 (0), 455–464.
Zhan, C.-s., Song, X.-m., Xia, J., Tong, C., 2013. An efficient integrated approach for global sensitivity analysis of hydrological model parameters. Environ. Model. Softw. 41 (0), 39–52.
Zonneveld, J., Golding, M., Moslow, T., Orchard, M., Playter, T., Wilson, N., 2011. Depositional framework of the lower triassic Montney Formation, west-central Alberta and northeastern British Columbia. Presented at the CSPG CSEG CWLS Convention: Recovery, Calgary, Alberta, Canada, 9–12 May.

Glossary

AF: Acentric factor
Bar sign "": Average value
C: Total number of components in the total composition misfit
CCE: Constant Composition Experiment
CGR: Condensate Gas Ratio
CR: Cross-over probability
DE: Differential Evolution
DFIT: Diagnostic fracture injection test
$\boldsymbol{E}$*:* Expected value
$f(\boldsymbol{x})$*:* Misfit value from reservoir simulation of vector **x**
$f(\boldsymbol{y})$*:* Misfit value from reservoir simulation of vector **y**
F: Step size or scaling factor
$^{\circ}F$*:* Degree Fahrenheit
h: Reservoir thickness, ft
k_f*:* Current fracture permeability, md
k_i*:* Original (initial) fracture permeability, md
KB: Kelly Bushing
l: Lateral length, ft
L: The width of the SRV in a 1D Model, ft
LRS: Liquid Rich Shale
m: Molar fraction
MARS: Multi-variate Adaptive Regression Spline
MFHW: Multi-Fractured Horizontal Well
MW: Molecular Weight
n_d*:* The dimension of problem
N_p*:* The number of members in an initial population of DE
p: Current pressure, psi
p_i*:* Initial pressure, psi
P_c*:* Critical pressure
PR-EOS: Peng–Robinson Equation of State
q: Production flow rate, bbl/Day (Liquid) or MMscf (gas)
Q_1, Q_2, Q_3*:* 25%, 50% and 75% quantiles
Q_{w_r}*:* Remaining water in the reservoir after injection, ft^3
$\boldsymbol{r}$*:* A random vector
r_i*:* Each member of **r** that is a random number between 0 and 1
R: A random index between 1 and n_d
RMS: Root Mean Square
RSM: Response Surface Model
S_{Ti}*:* Total order Sobol' indices
S_{w_init}*:* Initial water saturation in the model
S_{w_SRV}*:* Initial water saturation in the SRV
SAGD: Steam Assisted Gravity Drainage
SG: Specific Gravity
SRV: Stimulated Reservoir Volume
T: Total number of timesteps
TVD: True Vertical Depth
T_b*:* Boiling temperature
T_c*:* Critical temperature
$\boldsymbol{v}_{G+1}$*:* Mutant vector
$\boldsymbol{V}$*:* Variance
V_c*:* Critical volume
w: Fracture width, ft
$\boldsymbol{x}$*:* A target vector from current population G
x_f*:* Fracture half length, ft
X: An uncertain input (model parameter)
$\boldsymbol{y}$*:* A crossed-over and mutated vector (outcome of DE)
$\boldsymbol{y}_{2,G}$ & $\boldsymbol{y}_{3,G}$*:* Two randomly selected distinct vectors from current population G
$\boldsymbol{y}_{best,\,G}$*:* The best member of current population G with a lowest Misfit
Y: Total output (Misfit)

Subscripts

$_G$*:* Generation
$_{best}$*:* The best member of a DE population
$_{o,\,g,\,w}$*:* Oil, gas, water
$_{obs}$*:* Observed data
$_{sim}$*:* Simulation data
$_{\sim i}$*:* All parameters except i

Greek letters

γ*:* Fracture reduction factor
δ*:* Molar fraction of components in oil or gas
ζ*:* A random number between 0 and 1
φ*:* Porosity